Journal of Physics: Conference Series

PAPER • OPEN ACCESS

# Experimental Evidence for Wigner's Tunneling Time

To cite this article: N Camus *et al* 2018 *J. Phys.: Conf. Ser.* **999** 012004





IOP Conf. Series: Journal of Physics: Conf. Series **999** (2018) 012004 doi:10.1088/1742-6596/999/1/012004

# Experimental Evidence for Wigner's Tunneling Time

**N Camus [1], E Yakaboylu[1,2], L Fechner[1], M Klaiber[1], M Laux[1], Y Mi[1], K Z Hatsagortsyan[1], T Pfeifer[1], C H Keitel[1], and R Moshammer[1]**

1 Max Planck Institute for Nuclear Physics, Saupfercheckweg, 1, Heidelberg, Germany
2 IST Austria, Am Campus 1, Klosterneuburg, Austria

E-mail: nicolas.camus@mpi-hd.mpd.de

**Abstract.** Tunneling of a particle through a barrier is one of the counter-intuitive properties of quantum mechanical motion. Thanks to advances in the generation of strong laser fields, new opportunities to dynamically investigate this process have been developed. In the so-called attoclock measurements the electron's properties after tunneling are mapped on its emission direction. We investigate the tunneling dynamics and achieve a high sensitivity thanks to two refinements of the attoclock principle. Using near-IR wavelength we place firmly the ionization process in the tunneling regime. Furthermore, we compare the electron momentum distributions of two atomic species of slightly different atomic potentials (argon and krypton) being ionized under absolutely identical conditions. Experimentally, using a reaction microscope, we succeed in measuring the 3D electron momentum distributions for both targets simultaneously. Theoretically, the time resolved description of tunneling in strong-field ionization is studied using the leading quantum-mechanical Wigner treatment. A detailed analysis of the most probable photoelectron emission for Ar and Kr allows testing the theoretical models and a sensitive check of the electron initial conditions at the tunnel exit. The agreement between experiment and theory provides a clear evidence for a non-zero tunneling time delay and a non-vanishing longitudinal momentum at this point.

## 1. Introduction

Modern laser technology can provide electric fields comparable to those electrons experience in atoms [1], opening opportunities to investigate the quantum-dynamical process of electron tunneling through the potential barrier formed by the superposition of both laser and atomic fields [2] (Fig. 1 a). Attosecond-time [3] and Ångström-space resolution of the strong laser-field technique [4] allow to address fundamental mechanisms related to tunneling, which are still open and debated[5, 6, 7, 8, 9]: What time is spent under the barrier and what momentum is picked up by the particle in the meantime? While these questions address the fundamental question how the electron transition occurs from the (quantum) bound state to the (quasi classically detected) continuum via the tunneling through the barrier, it has also relevant applications for attosecond spectroscopy because common techniques such as high-harmonic generation [10, 11] or laser-induced electron diffraction [12, 13] rely also on tunnel ionization.

To specifically probe the tunneling step one takes advantage of the fact that the electron, once ionized, is driven by the laser electric field. Using close-to-circularly polarized laser pulses, and therefore a rotating electric field, the instant of time when the electron appears in the continuum is effectively mapped onto a characteristic emission direction that can be measured after the pulse (attoclock configuration) [3, 14, 15, 6]. However, in order to gain a meaningful

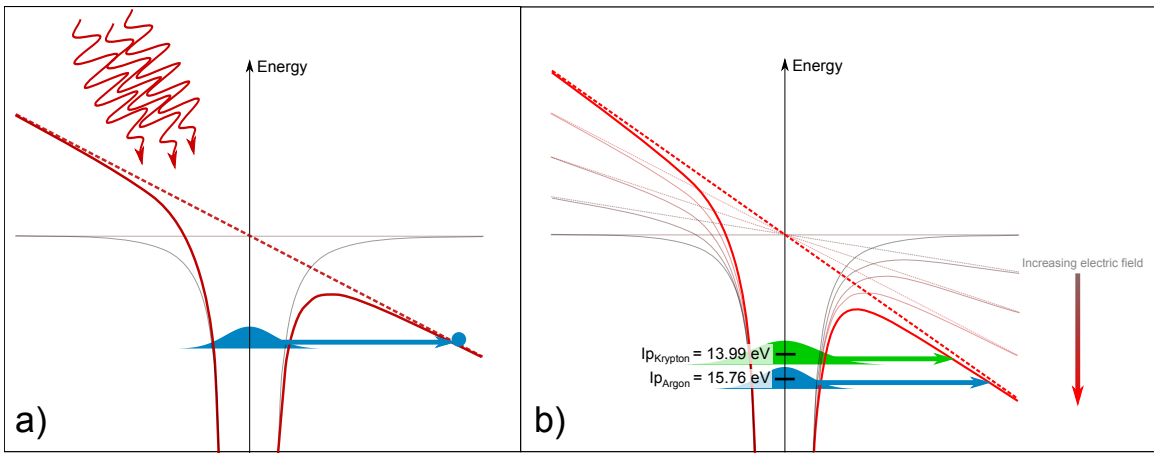


**Figure 1.** a) Schematic representation of the tunneling ionization: the Coulomb potential is bent by the laser electric field forming a barrier in the potential. The bound electron wave packet is ionized through tunneling and considered to appear as a classical particle at the tunnel exit. b)Scheme to attain a high sensitivity on the barrier influence in tunneling ionization: comparing two atomic species with similar ionization potential.

interpretation of the tunneling step (time, momentum, and position right after tunneling) by inspection of the final photoelectron momentum distribution, the laser pulse parameters must be known and the Coulomb interaction with the remaining ion along the electron excursion in the continuum must be taken into account. Moreover, the Coulomb field effect depends itself on the initial conditions and cannot be evaluated independently. These considerations lead to an ongoing debate about the role of the initial electron momentum [16, 5, 17, 18, 19] as well as the question whether and how the electron motion can be traced back to the tunneling step [15, 6, 8].

Our strategy to achieve a high sensitivity on the tunneling step is to compare strong-field tunneling ionization of atomic species with slightly different ionization potentials (argon and krypton), but under otherwise absolutely identical laser fields (Fig. 1 b). We therefore effectively reduce the influences of other effects such as differences in Stark shifts, atom polarizabilities, dependences on the initial-state orbital momentum [16], and systematic experimental errors, as well as reduce the effect of the Coulomb field. Similarly to other attoclock investigations, we vary in addition the laser intensity such that we can investigate a large range of effective tunneling barrier widths.

Experimentally, we simultaneously collect within the same experiment photoelectron momentum distributions with high resolution for ionization of a gas mixture containing argon and krypton. Using a Reaction Microscope spectrometer that allows for the coincident detection of electron-ion pairs created by ionization of Ar or Kr atoms,we can compare the spectra obtained otherwise under the same laser and experimental conditions. The experimental results allow for a stringent test of theoretical predictions. Our theoretical model is based on the assumption that the electron dynamics is quasiclassical when the electron distance from the tunnel exit exceeds a few de-Broglie wavelengths. The tunneling dynamics is described quantum mechanically via numerical solution of the Schrödinger equation, assuming that the barrier is quasistatic during the brief time of the tunneling. The important point is the matching of the quantum mechanical and classical dynamics. The latter is accomplished employing a quantum trajectory method, which is a generalization of the Wigner concept of the scattering time delay [20]. The quantum trajectory or the Wigner trajectory is derived from the exact wave function. It starts from an

under the barrier point and further propagates in the continuum, coinciding with a classical trajectory slightly away from the tunnel exit, and provides the initial conditions for the specific classical trajectory in the continuum. Further classical dynamics in the laser and Coulomb fields yields the asymptotic photoelectron momentum. In this way we deduce the signatures of the tunneling step from the asymptotic photoelectron momentum distribution.

## 2. Experimental setup

### *2.1. Reaction Microscope spectrometer*

To study the electron momentum distributions for ionization of two atomic systems (argon and krypton) with slightly different ionization potentials $I_p$ within the same experiment we make use of the coincidence capability of the reaction microscope (Fig. 2). By doing such we can avoid the intrinsic experimental inaccuracies of independent measurements (changes in the laser properties and systematic uncertainties).

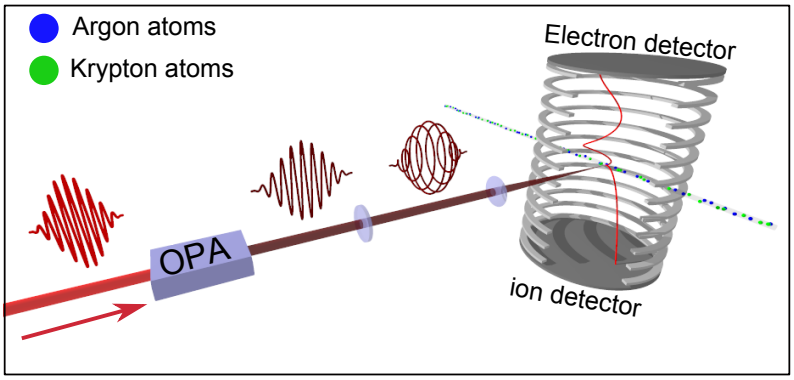


**Figure 2.** Experimental setup: close to circularly polarized laser pulses with a 1300 nm wavelength are focused onto a gas mixture of argon and krypton inside a reaction microscope.

Linearly polarized 1300 nm radiation was generated by an optical parametric amplification (OPA) system (TOPAS-C, Light Conversion) pumped by 25 fs, 790nm pulses from a Ti:Sapphire based laser system. The ellipticity, using broadband waveplates, was determined to be 0.85 $\pm$ 0.05 (the ratio of the minor to the major axis). The laser intensity at the target was adjusted using a motorized iris. The laser pulses are focused onto a supersonic, internally cold gas jet inside a Reaction Microscope (ReMi). The reaction fragments (electrons and ions) are guided by weak homogeneous electric and magnetic fields onto time and position sensitive detectors. From their times of flight and their impact positions, the initial momentum vectors of the fragments are determined [21, 22].

### *2.2. Observables*

In Fig. 3a) the measured electron momentum distributions for argon and krypton for a laser intensity of about $2 \times 10^{14} W/cm^2$ are shown. As expected for atoms with similar ionization potentials, the spectra for both targets appear almost identical. However, clear differences manifest when looking at the difference spectrum of the normalized distributions (Fig. 3a) right panel).

As developed in the theory section below, the value of interest is the most probable electron trajectory, in particular the final momentum and the angle of rotation with respect to the axes of the polarization ellipse [14]. This correspond to the angle $\theta_{max}$ of the distribution where the number of counts is maximum. $\theta_{max}$ is the observable that is most sensitive to both time delay

and initial momentum. In the present case we focus on the angle difference $\Delta\theta_{max} = \theta^{Ar}_{max} - \theta^{Kr}_{max}$ as a function of intensity.

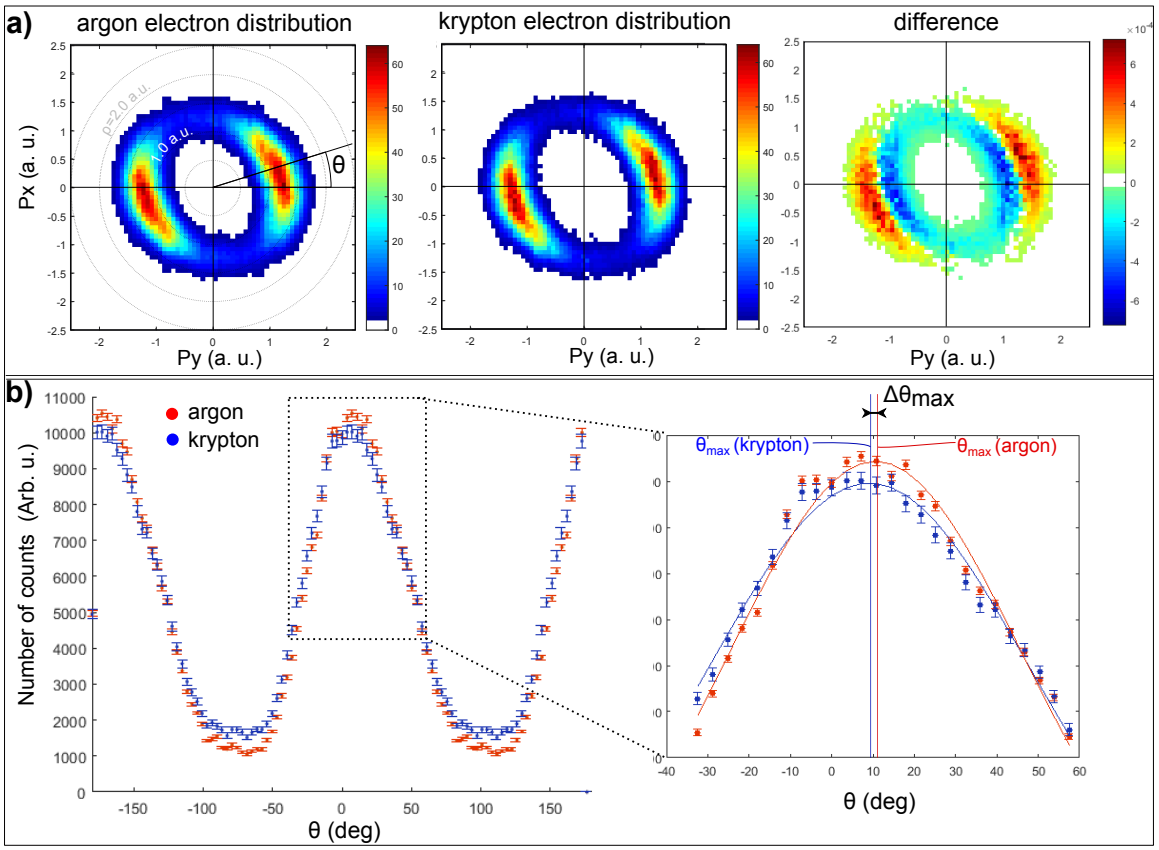


**Figure 3.** a) Momentum distribution of argon (left), krypton (middle) and the difference (right). b) Angular distribution for argon (red) and krypton (blue). Adapted from [23].

In a strong-field experiment it is almost impossible to measure with high accuracy the absolute value of the intensity since the interaction point is placed in a close vacuum chamber. Instead, the intensity is usually calibrated by comparing the photoelectron and photoion distributions with theory [24]. In the case of the attoclock experiment, the conversion between intensity and radius of the 2D momentum distribution is actually debated [25, 26]. To prevent from any bias, we choose to use the average electron momentum at $\theta_{max}$ for ionization of argon: $\rho(\theta_{max}) = \rho^{Ar}(\theta_{max}) = \sqrt{p_x^{Ar}(\theta_{max})^2 + p_y^{Ar}(\theta_{max})^2}$. For circularly and elliptically polarized pulses this average momentum $\rho(\theta_{max})$ is an unambiguous measure of the actual intensity.

The resulting curve $\Delta\theta_{max}$ as a function of $\rho(\theta_{max})$ is plotted in comparison with our theoretical model in Fig. 7.

## 3. Theoretical model

We develop a model where the tunneling ionization step is treated in the Wigner formalism and the results provided by these calculations are used as initial conditions for a classical propagation of the electron in the continuum.

*3.1. Wigner trajectory*

The quantum mechanical description of the propagation of the ionized electron is given by the propagation of the wave function

$$\Psi(\boldsymbol{r},t) = \langle \boldsymbol{r}|U(t,t_s)|\Psi(t_s)\rangle = \int d\boldsymbol{r}_i\, K(\boldsymbol{r},\boldsymbol{r}_i;t,t_s)\Psi(\boldsymbol{r}_i,t_s)\,, \tag{1}$$

where $\Psi(\boldsymbol{r}_i,t_s)$ is the initial wave function, and the term $K(\boldsymbol{r},\boldsymbol{r}_i;t,t_s) = \langle \boldsymbol{r}|U(t,t_s)|\boldsymbol{r}_i\rangle$ is the corresponding space-time propagator which connects space points $\boldsymbol{r}_i$ and $\boldsymbol{r}$ in a time interval $t-t_s$.

The adiabaticity of the ionization process is guaranteed by a small Keldysh parameter($\gamma < 1$) for most of the parameter regime under consideration here. We can therefore assume that the energy is conserved during the process, and accordingly the space-time propagator can be written in terms of the fixed-energy propagator $G(\boldsymbol{r},\boldsymbol{r}_i,\varepsilon)$, the retarded Green's function of the Time Independent Schrödinger Equation (TISE). After mapping the three-dimensional geometry onto a one-dimensional tunneling geometry in parabolic coordinates [5], the space-time propagator is written as

$$K(\eta,\eta_i,t-t_s) = \frac{1}{2\pi}\int_{-\infty}^{\infty} d\varepsilon\, e^{-i\varepsilon(t-t_s)} G(\eta,\eta_i,\varepsilon)\,, \tag{2}$$

where the Green's function is given by

$$\left(\frac{\varepsilon}{4} + \frac{1}{2}\frac{\partial^2}{\partial\eta^2} - V_B(\eta)\right) G(\eta,\eta_i,\varepsilon) = \delta(\eta-\eta_i)\,. \tag{3}$$

Decomposing the Green's function into its phase and amplitude, by means of the stationary phase analysis we deduce that solutions of the equation

$$(t-t_s) - \frac{\partial \arg\left[G(\eta,\eta_i,\varepsilon)\right]}{\partial\varepsilon} = 0 \tag{4}$$

yield the dominant energies. In other respect, as in the case of tunnel-ionization, if the ionization energy is the dominant energy then the trajectory

$$t(\eta,\eta_i) = \left.\frac{\partial \arg\left[G(\eta,\eta_i,\varepsilon)\right]}{\partial\varepsilon}\right|_{\varepsilon=-I_p} + t_s \tag{5}$$

is the dominant trajectory for the space-time propagator.

We name it Wigner trajectory as it generalizes the Wigner approach for the scattering time delay [20] to the tunneling problem. In the original idea of Wigner the asymptotic time delay at scattering was described by the derivative of the scattering phase shift with respect to energy. The definition of the dominant trajectory is quite natural. In fact, in the WKB approximation, the phase corresponds to the classical action, hence the definition of a trajectory by Eq. (5) would follow the Hamilton-Jacobi theory (see for instance Ref. [27]). In the quantum domain the Wigner trajectory corresponds to the maximum of the electron probability current density [28].

In the case of a one-dimensional problem the Green's function can be calculated:

$$G(\eta,\eta_i,\varepsilon) = \frac{2i}{W}\left[\theta(\eta-\eta_i)\psi_+(\eta,\varepsilon)\psi_-(\eta_i,\varepsilon) + \theta(\eta_i-\eta)\psi_-(\eta,\varepsilon)\psi_+(\eta_i,\varepsilon)\right] \tag{6}$$

with $W = \psi_-(\eta,\varepsilon)\partial_\eta\psi_+(\eta,\varepsilon) - \psi_+(\eta,\varepsilon)\partial_\eta\psi_-(\eta,\varepsilon)$ being the Wronskian [29, 30, 31], where $\psi_+(\eta,\varepsilon)$, and $\psi_-(\eta,\varepsilon)$ are the corresponding solutions of the TISE

$$\left(-\frac{1}{2}\frac{d^2}{d\eta^2} + V_B(\eta)\right)\psi_\pm(\eta,\varepsilon) = \frac{\varepsilon}{4}\psi_\pm(\eta,\varepsilon) \tag{7}$$

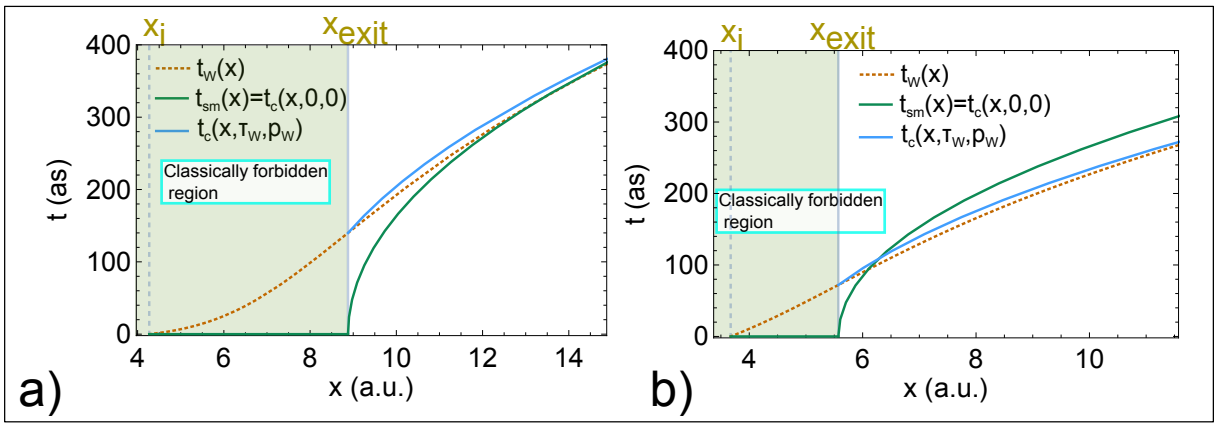


**Figure 4.** Electron trajectories in different models at low (a) and high (b) laser intensities: (dashed, orange) Wigner trajectory via Eq. (5), (green, solid) the simple-man trajectory, (blue, solid) classical trajectory with the initial conditions given by the Wigner formalism. The trajectories are calculated for a krypton atom. The laser intensities are $I = 1.7$ (a) and $I = 6.1 \times 10^{14}$ W/cm$^2$ (b). The trajectories are shown in one-dimensional (along the tunneling direction) Cartesian coordinate. Adapted from [23].

with positive and negative current, respectively. The phase of the Green's function is written as

$$\arg\left[G(\eta, \eta_i, \varepsilon)\right] = S_+(\eta, \varepsilon) - S_+(\eta_i, \varepsilon)\,, \quad \eta \geq \eta_i\,, \tag{8}$$

where $S_\pm \equiv \arg(\psi_\pm)$, and we use the fact that $S_-(\eta_i, \varepsilon) = -S_+(\eta_i, \varepsilon)$. The Wigner trajectory is then defined by the phase of the TISE wave function with a positive outgoing probability current

$$t_W(\eta, \eta_i) = \frac{\partial S(\eta, -I_p)}{\partial \varepsilon} - \frac{\partial S(\eta_i, -I_p)}{\partial \varepsilon} + t_s\,, \tag{9}$$

where we omit the sub-index + for the phase $S_+$. The initial coordinate $\eta_i$ corresponds to the position where the tunneling part of the wave packet is maximum at $t_s$. The initial $\eta_i$ value are found solving numerically the time dependent Schrödinger equation in parabolic coordinates. They correspond to the saddle point of the potential.

Transforming back to Cartesian coordinates, we show the Wigner trajectories for the two different regimes, low and high intensity in Fig. 4.

We observe that in both regimes the electron spends a finite time under the barrier until it reaches the exit and it is set into the continuum with a positive time delay $\tau_W \equiv t_W(x_{exit}) > 0$ (see the orange dotted curves in Fig. 4). We also observe a nonvanishing longitudinal momentum along the laser field direction at the tunnel exit $p_W = \left(d\, t_W(x)/dx\right)^{-1}|_{x=x_{exit}}$. This is in agreement with previous observations of the dominant trajectories using a somewhat simpler potential [7, 32].

### *3.2. Classical propagation*

To connect the tunneling step with the subsequent electron motion in the classically allowed region during the second step, we define a classical trajectory starting at the tunnel exit $x_{exit}$ at time $t_{exit} = \tau_W$ with an initial momentum $p_{exit} = p_W$ (Fig. 4 blue curves). As the laser field rotates during the tunneling time delay, the electron emission direction as well as the position of the tunnel exit are adapted to the field direction after the time delay $\tau_W$. The final electron

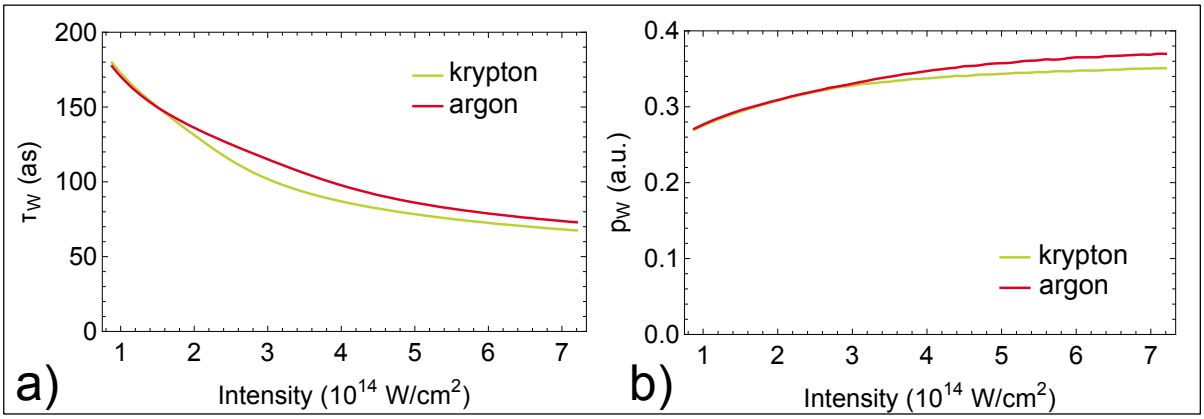


**Figure 5.** Initial conditions arising from the Wigner formalism for the two investigated atoms (argon and krypton): initial time (a) and initial longitudinal momentum (b). Notably, at the tunnel exit, the differences between both targets, argon and krypton, are as small as 10 attoseconds for the time delay and less than 0.1 a.u. for the longitudinal momentum. Adapted from [23].

momentum after the laser pulse is calculated via classical propagation

$$\boldsymbol{p}_f = \boldsymbol{p}_{exit} - \int_{t_{exit}}^{\infty} dt\ [\boldsymbol{E}(t) + \nabla U(\boldsymbol{r}(t))]\ , \tag{10}$$

by solving Newton's equations of motion $\ddot{\boldsymbol{r}}(t) = -\nabla U(\boldsymbol{r}(t)) - \boldsymbol{E}(\boldsymbol{t})$, with $\boldsymbol{E}(t)$ being the laser electric field and $U(\boldsymbol{r})$ the potential of the atomic core taking into account its polarization by the laser [33].

How the initial conditions affect the asymptotic electron momentum is shown fig. 4 where we compare the trajectory using the Wigner initial condition $t_c(x, \tau_W, p_W)$ (green curve) with the trajectory of the commonly used classical simple-man (SM) model $t_{sm}(x)$. The latter is defined having a zero delay time and zero initial velocity at the tunnel exit. By neglecting the atomic Coulomb potential in the SM model, the final momentum becomes $\boldsymbol{p}_f = -\int_{t_0}^{\infty} dt\, \boldsymbol{E}(t)$ and quantitative information can be derived. A tunneling time delay corresponds to a rotation of the asymptotic momentum distribution by $\delta\theta_\tau = \omega\tau_W$, and the non-zero initial momentum to a counter-rotation by $\delta\theta_p \approx -p_w/p_E$ with $p_E = E_0/\omega$, with $\omega$ and $E_0$ being the laser-field frequency and amplitude, respectively. For low intensities, one compensates the other almost perfectly and the SM trajectory merge asymptotically with the Wigner one. However for larger intensities the Wigner time delay decreases faster than the initial momentum increases. This leads to an additional net rotation compared to the SM prediction $\delta\theta = \delta\theta_\tau - \delta\theta_p$.

## 4. Comparison between experiment and theory

In Fig. 5 we show the time delay and initial momentum obtained from the Wigner formalism as a function of intensity for each target. These conditions are used to compare with experimental results over a large intensity span.

However, in order to compare experiment and theory, we need to identify for the theory, which pulse parameters should be used (pulse duration, shape and ellipticity) since these parameters are determined in the experiment with a limited accuracy. For these we make use of two additional observables dependent on the laser interaction: the difference in average radius $\rho_{Ar} - \rho_{Kr}$ and the yield ratio $Yield_{Ar} - Yield_{Kr}$ and analyze them as a function of intensity (Fig. 6). We

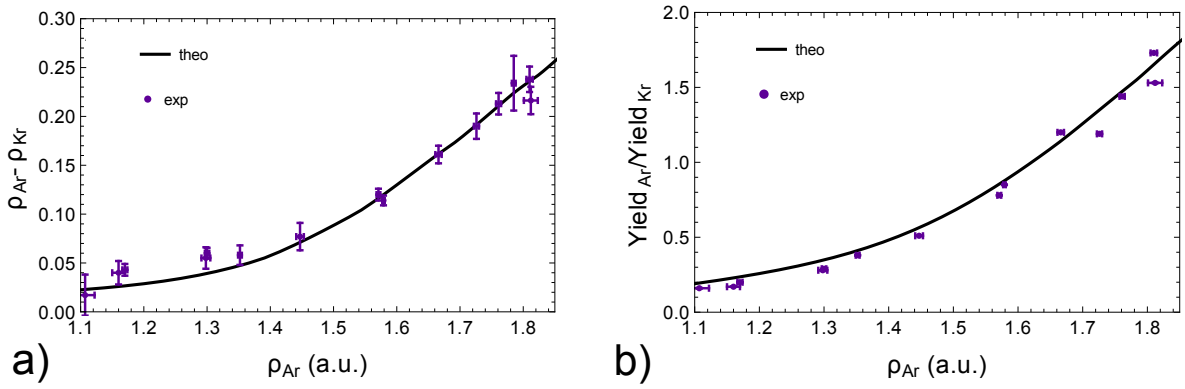


**Figure 6.** Comparison of the experiment and the theory; a) the difference between the average electron momentum, b) the yield ratio. Adapted from [23].

extract the pulse parameters which give the best agreement between theory and experiment for these two observables.

With these parameters for the theory we compare the angle difference between argon and krypton as shown in Fig. 7. We note that the only differences between the two theoretical curves in Fig. 7 are the chosen combinations for the initial momentum and the Wigner time. We conclude that the simple-man model (the dashed curve) fails to predict the experimental data whereas the solid curve, whose initial conditions are given by the Wigner formalism, agrees well with the experiment in the regime where $\rho_{Ar} \geq 1.3 a.u.$ [23]. In the low intensity domain ($\rho_{Ar} < 1.3 a.u.$) one has to take into account non-adiabatic effects to tunnel-ionization such as non-adiabatic momentum shifts [34], and tunnel exit shifts [18]. This is the domain where the Wigner formalism converges to the simple-man model because the Keldysh parameter approaches unity.

The agreement remains even if slightly different parameters are used (pulse shape, pulse duration, ellipticity). There is no scenario with the initial time and momentum set to zero which can reproduce the observed angular distribution. The variation of pulse parameters has almost no influence on the main observable $\Delta(\theta_{max})$.

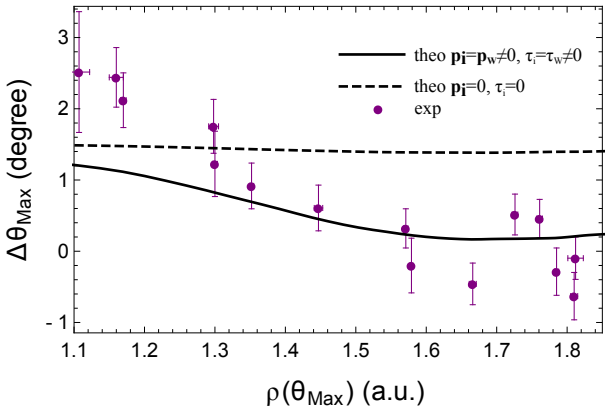


**Figure 7.** Difference between the most probable photoelectron emission angle for argon and krypton. Experiment and theory (with and without initial momentum and tunneling delay time). Adapted from [23].

## 5. Conclusion

We have investigated the quasi-classical description of strong-field tunneling ionization. Based on the Wigner formalism we identify the tunneling delay time and the initial longitudinal momentum at the tunnel exit for the most probable trajectory of the tunneling electron and test this formalism by comparison to the experiment. We show that the experimental results can be reproduced only when nonvanishing values for these parameters are used.

## References

[1] Brabec T and Krausz F 2000 *Rev. Mod. Phys.* **72** 545–591
[2] Keldysh L V 1965 *JETP* **47** 1307
[3] Eckle P, Pfeiffer A N, Cirelli C, Staudte A, Dörner R, Muller H G, Büttiker M and Keller U 2008 *Science* **322** 1525–1529
[4] Krausz F and Ivanov M 2009 *Rev. Mod. Phys.* **81**(1) 163–234
[5] Pfeiffer A N, Cirelli C, Landsman A S, Smolarski M, Dimitrovski D, Madsen L B and Keller U 2012 *Phys. Rev. Lett.* **109**(8) 083002
[6] Landsman A S, Weger M, Maurer J, Boge R, Ludwig A, Heuser S, Cirelli C, Gallmann L and Keller U 2014 *Optica* **1** 343–349
[7] Yakaboylu E, Klaiber M and Hatsagortsyan K Z 2014 *Phys. Rev. A* **90**(1) 012116
[8] Ni H, Saalmann U and Rost J M 2016 *Phys. Rev. Lett.* **117**(2) 023002
[9] Torlina L, Morales F, Kaushal J, Ivanov I, Kheifets A, Zielinski A, Scrinzi A, Muller H G, Sukiasyan S, Ivanov M and Smirnova O 2015 *Nature Phys.* **11** 503–508
[10] Corkum P B and Krausz F 2007 *Nature Phys* **3** 381
[11] Calegari F, Sansone G, Stagira S, Vozzi C and Nisoli M 2016 *J. Phys. B* **49** 062001
[12] Meckel M, Comtois D, Zeidler D, Staudte A, Pavičić D, Bandulet H C, Pépin H, Kieffer J C, Dörner R, Villeneuve D M and Corkum P B 2008 *Science* **320** 1478–1482
[13] Blaga C I, Xu J, DiChiara A D, Sistrunk E, Zhang K, Agostini P, Miller T A, DiMauro L F and Lin C D 2012 *Nature* **483** 194–197
[14] Eckle P, Smolarski M, Schlup P, Biegert J, Staudte A, Schöffler M, Muller H G, Dörner R and Keller U 2008 *Nature Phys.* **4** 565–570
[15] Pfeiffer A N, Cirelli C, Smolarski M, Dimitrovski D, Abu-samha M, Madsen L B and Keller U 2012 *Nature Phys* **8** 76–80
[16] Barth I and Smirnova O 2011 *Phys. Rev. A* **84**(6) 063415
[17] Li M, Liu Y, Liu H, Ning Q, Fu L, Liu J, Deng Y, Wu C, Peng L Y and Gong Q 2013 *Phys. Rev. Lett.* **111**(2) 023006
[18] Klaiber M, Hatsagortsyan K Z and Keitel C H 2015 *Phys. Rev. Lett.* **114**(8) 083001
[19] Li M, Geng J W, Han M, Liu M M, Peng L Y, Gong Q and Liu Y 2016 *Phys. Rev. A* **93**(1) 013402
[20] Wigner E P 1955 *Phys. Rev.* **98**(1) 145–147
[21] Ullrich J, Moshammer R, Dorn A, Dörner R, Schmidt L P H and Schmidt-Böcking H 2003 *Reports on Progress in Physics* **66** 1463
[22] De Jesus V, Rudenko A, Feuerstein B, Zrost K, Schröter C, Moshammer R and Ullrich J 2004 *Journal of electron spectroscopy and related phenomena* **141** 127–142
[23] Camus N, Yakaboylu E, Fechner L, Klaiber M, Laux M, Mi Y, Hatsagortsyan K Z, Pfeifer T, Keitel C H and Moshammer R 2017 *Phys. Rev. Lett.* **119**(2) 023201
[24] Alnaser A S, Tong X M, Osipov T, Voss S, Maharjan C M, Shan B, Chang Z and Cocke C L 2004 *Phys. Rev. A* **70**(2) 023413
[25] Ivanov I A and Kheifets A S 2014 *Phys. Rev. A* **89**(2) 021402
[26] Boge R, Cirelli C, Landsman A S, Heuser S, Ludwig A, Maurer J, Weger M, Gallmann L and Keller U 2013 *Phys. Rev. Lett.* **111**(10) 103003
[27] Schulman L S 2012 *Techniques and applications of path integration* (Dover Publications)
[28] Teeny N, Yakaboylu E, Bauke H and Keitel C H 2016 *Phys. Rev. Lett.* **116**(6) 063003
[29] Byron F W and Fuller R W 1992 *Mathematics of classical and quantum physics* (New York,: Dover Publications Inc.)
[30] Arfken G B 2013 *Mathematical methods for physicists* (New York: Academic press)
[31] Morse P and Feshbach H 1953 *Methods of theoretical physics* International series in pure and applied physics (McGraw-Hill)
[32] Czirjk A, Kopold R, Becker W, Kleber M and Schleich W 2000 *Optics Communications* **179** 29 – 38
[33] Dimitrovski D, Martiny C P J and Madsen L B 2010 *Phys. Rev. A* **82**(5) 053404
[34] Mur V, Popruzhenko S and Popov V 2001 *Journal of Experimental and Theoretical Physics* **92** 777–788